Infrared Earth Tracking for Deep-Space Optical Communications—Laboratory Experiments

Y. Chen,[1] J. Charles,[1] H. Hemmati,[1] and A. Biswas[1]

We report on laboratory emulator experiments performed to assess the feasibility of infrared (IR) Earth image tracking for optical communications. A quantum-well infrared photodetector (QWIP) is evaluated and characterized for this purpose. For proof of concept, an emulator is designed and implemented in the laboratory to generate IR Earth images over the range of 0.38 to 40 AU at the focal-plane array of the QWIP camera to evaluate the feasibility of using IR Earth images as optical communication pointing references. IR Earth images measured from the test-bed emulator are compared with the corresponding images derived from Earth thermal modeling, and the two are found to be in good agreement. IR Earth image nonuniformity is also emulated in the laboratory test bed, demonstrating that for characteristic deep-space optical apertures, the image is dominated by the Earth thermal nonuniformity at short distances (<2 AU) but is overwhelmed by diffraction blurring beyond 4 AU. Preliminary laboratory test-bed emulator investigation on centroiding accuracy of IR Earth center detection shows improved centroiding accuracy with increasing image size and IR signal level.

I. Introduction

The narrow beam width of laser communication beams necessitates accurate beam pointing. Laser beam pointing with an accuracy of hundreds of nanoradians is required for optical communications from deep space. In conjunction with proper inertial reference, a flight laser communication transceiver acquiring beam-pointing knowledge from a reliable beacon reference may meet such a requirement. The beacon can be a laser beam transmitted from Earth, the Sun-illuminated Earth, or other celestial bodies, such as stars. Among these options, only the laser-beacon tracking has been demonstrated from near-Earth space-based platforms.

In addition to overcoming the atmospheric-turbulence-induced degradation of the laser beam propagating to space, the required laser-beacon power has to be high in order to extend reliable tracking into deep space. For example, the beacon power needed to cover communication distances applicable to Mars with a laser transmitted from a ground-based telescope can be as much as 0.5 kW [1]. Beyond Jupiter, implementation of sufficient laser beacon power becomes very challenging. Apart from the excessive power level demand for long-range missions, a high-power uplink laser raises safety issues for airborne

[1] Communications Architectures and Research Section.

The research described in this publication was carried out by the Jet Propulsion Laboratory, California Institute of Technology, under a contract with the National Aeronautics and Space Administration.

and space-borne assets. Therefore, operation of a high-power laser beacon must comply with relevant regulations. For optical communications to the far reaches of deep space, operation safety and cost are major constraints of laser-beacon tracking.

Considering the limitations of a laser beacon, an Earth image sensed in long-wavelength infrared is an attractive option for establishing optical links between spacecraft and Earth [2]. IR Earth tracking provides the potential to extend the precision tracking of Earth's location over the entire solar system and beyond. In the visible region, crescent Earth and Earth albedo variations make the Earth tracking difficult. An IR Earth image, shown in Fig. 1, has much less variation and provides the potential to eliminate the need for a laser beacon for an outer planetary mission.

Figure 1 presents Earth images taken by the Mars Odyssey spacecraft in April 2001 from a range of 3.56 million km. The visible (reflected sunlight) band image shows only a thin crescent Earth, whereas in an infrared band emission between 8 and 13 μm a full Earth thermal image was observed. Further, in the infrared there is little phase variation. The emissivity nonuniformity of Earth thermal images is also comparatively small (6 to 1) because of slow thermal fluctuations of the Earth surface compared to more significant changes of reflectivity of the Earth in the visible wavelength (10,000 to 1). With a full image, the IR Earth center location can easily be identified from detecting its thermal radiation in the cold universe. Knowing the Earth center, the receiver location relative to the center of the Earth can be derived from time information and a terminal coordinate model.

The IR image of Earth is a promising beacon reference for providing the required beam-pointing accuracy for optical communications. Indeed, our preliminary theoretical analysis has indicated that IR Earth tracking can be used to cover the entire solar system up to 40 AU, meeting the required beam-pointing accuracy for optical communications [2]. To advance the concept of IR Earth tracking toward flight implementation, it is necessary to examine its feasibility both analytically and experimentally. For this purpose, a laboratory emulator was set up to simulate the IR Earth image through a range from 0.1 to 40 AU. The goal of the experimental setup is to investigate practical issues concerning IR Earth tracking, including (1) the effect of receiver optics emissivity from the receiving optical train, which is a dominant noise source; (2) blurring introduced by a finite telescope aperture; (3) point-ahead implementation; and (4) IR Earth image nonuniformity and its effect on centroiding accuracy. A major challenge for the emulator was small signal detection in a background environment that is warmer than the background of space behind the real Earth.

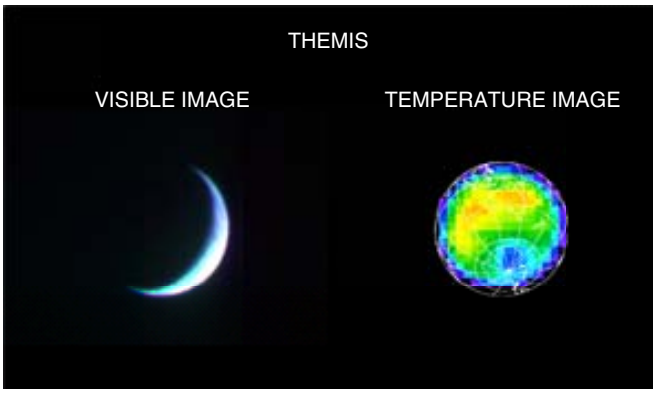

Fig. 1. A visisble Earth image (left) compared with the thermal image (right) taken by the Mars Odyssey spacecraft.

Given the relatively small apertures (10 to 50 cm) envisioned for a deep-space optical communication terminal, the IR Earth signal becomes very faint for an outer planetary mission. An IR camera onboard the spacecraft is an essential element for the IR Earth signal detection, particularly in regard to its sensitivity and noise feature. As a part of the IR Earth-tracking feasibility study in the laboratory, we have examined one type of IR camera, a quantum-well infrared photodetector (QWIP), extensively. Understanding available IR cameras and their characteristics helps the design of the IR Earth-tracking experiment and will also lay the groundwork for using IR Earth tracking in a future flight terminal implementation.

II. Laboratory Test-Bed Emulator Design and Layout

A test setup for emulating the Earth image, as it would appear on a flight transceiver focal plane, was designed and assembled. The emulator design accommodated terminal aperture diameters from 10 to 50 cm, deep-space distances ranging from 0.1 to 40 AU, and infrared wavelengths from 8 to 14 μm. To easily accommodate the wide range of wavelengths, an all-reflective emulator optical system was used. Furthermore, the means to account for emissivity nonuniformity was also introduced, as elaborated below.

A significant emphasis of the emulator architecture is to simulate the relative size of the Airy pattern of the receiver telescope with respect to the Earth image. For a given optical terminal aperture, the Airy pattern will always correspond to the same angular extent for a given wavelength. Since the angular size of Earth will clearly change with distance, the effect of the Airy pattern on the image of Earth will also change with distance, with the most profound influence occurring at greater distances. For a terminal aperture of 30 cm and a wavelength of 9 μm, the full width at half maximum (FWHM) of the Airy disk will exceed the imaged size of Earth at a range below 3 AU. At 30 AU, the FWHM will be more than 10 times larger than the Earth image, and the Earth approaches a point source.

A simplified schematic of the designed emulator setup is shown in Fig. 2. The emulator consists of an IR source emulating IR Earth emission, interchangeable range mirrors 1 to 8 for distance emulation in space, imaging mirrors 1 and 2 to mimic receiver telescope focal function, a telescope aperture emulator for simulating receiver telescope aperture size, and a receiver IR camera for the Earth image detection. To generate IR Earth-like emission, IR objects of various types and sizes may be used. In our setup, the most often used IR source had a circular emission area with a diameter of 22 mm. With a source of this size, the receiver needs to be placed far away to emulate Earth image sizes that can conform to a simulated distance up to 40 AU. For example, the Earth image size is 84 μrad at 1 AU. Implementation of such an emulation distance in a purely geometrical way requires the spacing between IR source and IR receiver to be 260 m, which is beyond practical realization on a laboratory bench. To overcome the laboratory spacing

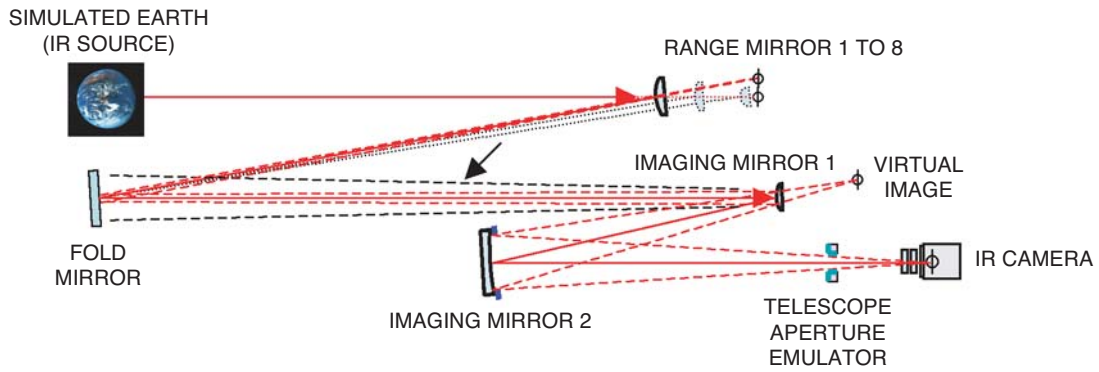

Fig. 2. The IR Earth-tracking laboratory emulator setup.

limitation and to generate Earth images at astronomical unit distances, convex spherical range mirrors 1 to 8, of varying radii, are included in the system. Setting the spacing between IR source and range mirrors (1 to 8) at 1.2 m and the spacing between range mirrors and imaging mirror 1 at 1 m (Fig. 2), eight range mirrors (1 to 8) produce emulated Earth distances of 0.38, 0.75, 1.5, 3, 6, 12, 24, and 48 AU, respectively. By varying the separations between IR source and range mirrors and between range mirrors and imaging mirror 1, the emulating distance can be varied continuously from 0.1 AU to beyond 40 AU on the laboratory test bed.

In a practical optical flight terminal, the IR Earth signal is received by a telescope with limited aperture size and focal length. The simulation of the telescope focal function is accomplished by imaging mirrors 1 and 2. Imaging mirror 1 is a convex spherical mirror with a radius of 336.7 mm, and imaging mirror 2 is a concave mirror with a radius of 1071.6 mm. The spacing between imaging mirror 1 and imaging mirror 2 is 700 mm. These two mirrors combined together yield the effective simulated telescope focal length of 5 m. The finite aperture size of the telescope is simulated by the iris on the test bed, identified by the telescope aperture emulator in Fig. 2. The iris can be opened completely for an effective 50-cm telescope aperture size and continuously reduced to emulate a telescope aperture size less than 5 cm.

The emulated IR Earth image is focused onto the detector array of the receiver IR camera by imaging mirrors 1 and 2. The detector array is placed at the focal point of the mirrors and is 1326 mm from imaging mirror 2. A PC computer is attached to the IR camera for data acquisition and processing.

III. IR Camera Characterization and Characteristics

The IR Earth signal, on a test bed or flight terminal, is captured by the receiver IR camera for signal processing and tracking. Obviously, the camera is a critical part of the IR Earth tracking and the laboratory test-bed experiment. Two IR cameras were used on the laboratory test bed and were characterized. One was a QWIP [3], which was developed by the Infrared Photonics Group at JPL and manufactured by Indigo. The other was a bolometer from Thermoteknix [4].

A. QWIP IR Camera

The QWIP camera has a spectral response in the 8- to 9.2-μm range, as shown in Fig. 3. This spectral response falls into peak irradiance in the 8- to 13-μm band of IR Earth emission for IR Earth tracking. The QWIP is cooled to 67 K with a Stirling cooler and has low dark current (1.5 pA at a bias voltage of -1.1 V) and low read noise (400 to 500 electrons). With its pixel well depth at 11 million electrons, the QWIP digitized 14-bit output renders 671 electrons per digital count. The camera has 640×512 pixels with a 25×25 μm^2 size for each pixel, yielding a field of view (FOV) of 63.2×52.4 deg for a 13-mm focal lens and 9.1×7.3 deg for a 100-mm focal lens, the two IR lenses we have.

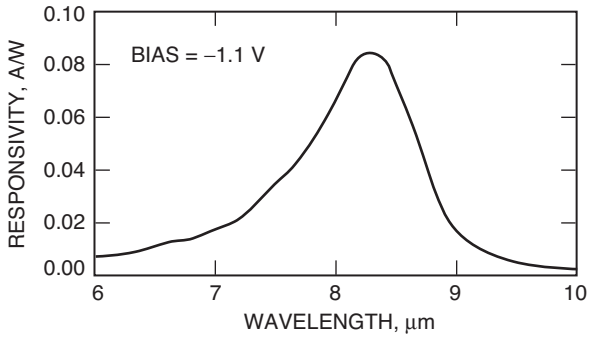

Fig. 3. The responsivity spectrum of QWIP.

The cooled camera's performance at low signal input is limited by pixel nonuniformity, dark current, and read noise. We examined the QWIP characteristics of nonuniformity, response to low temperature/signal level, saturation limitation, linearity versus integration time, and response to integrating sphere tests.

1. Pixel-to-Pixel Nonuniformity. Pixel-to-pixel nonuniformity can be a major source of noise that influences the signal response of a focal-plane array (FPA), especially at low and high signal levels. Figure 4 illustrates the measured nonuniformity—defined as the standard deviation of the pixel-to-pixel variation over a 400×400 pixel area in the middle of the detector array divided by the mean output—of the QWIP camera that was examined. Measurements are taken by using an integrating sphere with an IR source, which generates a uniform IR-illuminated level directly in front of the QWIP detector array. The point on the left side of Fig. 4 is a measurement taken without the integrating sphere, using liquid nitrogen for low signal input. The rest of the data points are acquired with the integrating sphere.

If the QWIP is calibrated across its 14-bit dynamic range and each calibration is applied to the corresponding input of signal flux level, pixel-to-pixel nonuniformity will be relatively small over its dynamic range.

The nonuniformity response of the QWIP focal-plane array has been measured to be ∼0.1 percent within the range where nonuniformity calibration was conducted, and no greater than 0.4 percent at high signal flux over a large portion of the array (400×400). The acceptable nonuniformity for the QWIP camera is expected to be 0.1 percent or less. Calibration across the dynamic range will reduce pixel-to-pixel nonuniformity to an acceptable level.

2. QWIP Response to Low Signal Input. The IR camera deployed for deep-space optical communications must be able to detect and adequately image the distant Earth. With the $1/R^2$ dependence, the IR Earth signal beyond Mars becomes very weak. It is especially important to understand the QWIP performance at low signal levels for its potential application in distant IR Earth imaging. To this end, the QWIP is examined for its response to low signal input. The experiment is conducted using liquid nitrogen held in a Styrofoam container. A cooled environment below −120 deg C is created over a large angular area covering the whole QWIP detector array. One of the QWIP images recorded with this liquid nitrogen arrangement is shown in Fig. 5.

Assuming perfect uniform pixel distribution and absence of noise (no dark current, read noise, negligible shot noise, etc.), the response of the QWIP to any flux input below −120 deg C at a 16-ms integration

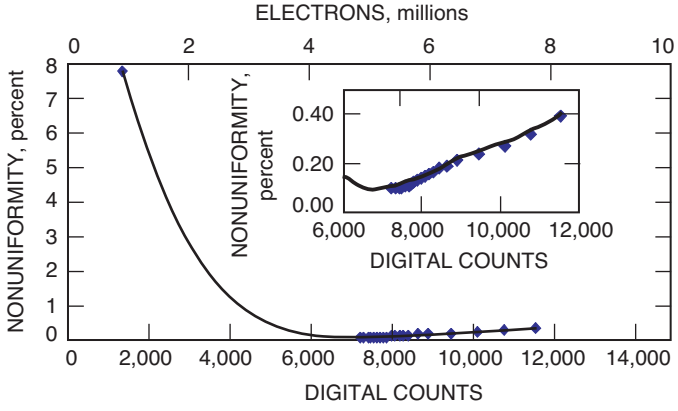

Fig. 4. Nonuniformity variation of the QWIP versus digital/electron counts with an integration time of 16 ms.

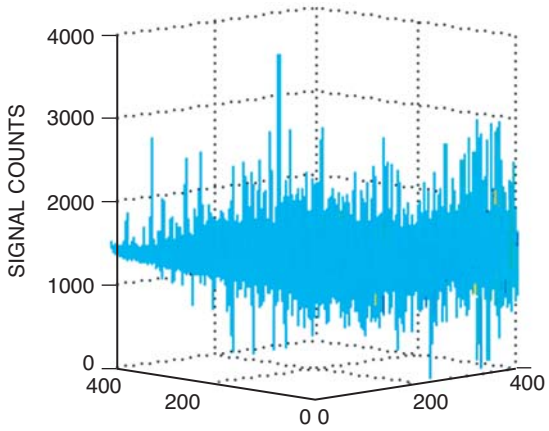

Fig. 5. The QWIP detector response for exposure to liquid nitrogen at a 16-ms integration time. Lateral units are numbers of pixels.

time should produce a zero-count output (based on the black body radiation theory). However, when exposed to a liquid nitrogen environment below −120 deg C, the QWIP detector produces a mean 1300-count output in a 14-bit data range (Fig. 5). This is due to the pixel-to-pixel nonuniformity of the camera. Within a 400×400 detector area, some individual pixels respond with a zero-count output while others get as high as over 3500 counts. By generating two uniform thermal signal levels in the ranges of −20 deg C and −40 deg C to calibrate the pixel-to-pixel nonuniformity at low temperatures, the nonuniformity limitation to low signal response can be overcome. Once the pixel-to-pixel nonuniformity limitation is alleviated, the dark current level of the QWIP camera can be observed and measured using liquid nitrogen.

3. Saturation Limitation. The QWIP camera has a large dynamic range to adapt to input signal flux variation. Its low-end range is limited by sensitivity to a small signal input. The high end is clipped by saturation at a large flux input. To clarify the limitation of the high end, an experiment is conducted on the QWIP output response versus the signal input variation. The IR source emission is directed toward the QWIP with a lens placed in its front, which focuses the signal on the focal-plane array. The emission level of the IR source is varied by adjusting the IR source emission temperature. The resulting output of the QWIP versus the input flux level is shown in Fig. 6.

Figure 6 indicates that the QWIP camera output mean counts increase with increased input signal flux in terms of the source emission temperature. At an integration time of 16 ms, the output starts to saturate near 80 deg C. The maximum output is limited to 14,500 counts or 9.7 million electrons. This output saturation below full well depth (11 million electrons, or 16,384 counts) results from pixel-to-pixel nonuniformity as well. The signal output counts plotted in Fig. 6 are averaged over the detector array. Although the average output can be, for example, 13,600 counts, individual pixels can reach full counts of 14 bits, as shown in Fig. 7. By calibrating pixel-to-pixel nonuniformity at a high flux input over the full dynamic range, this limitation of saturation can be extended to close to the full well depth of 11 million electrons.

4. Linearity versus Integration Time. To image input signals over a large range of flux variation, the QWIP also has an option to vary integration time, with a long integration time used for a low signal level and a short integration time used for a high signal level. The signal output at a fixed input

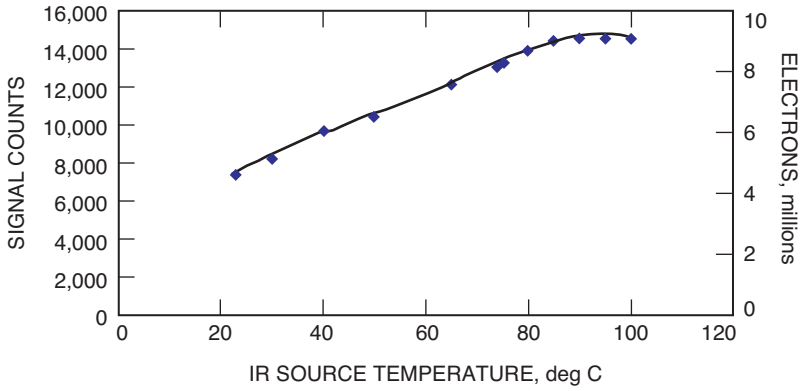

Fig. 6. The QWIP output of signal mean counts at a 16-ms integration time in response to variation of input IR source emission level.

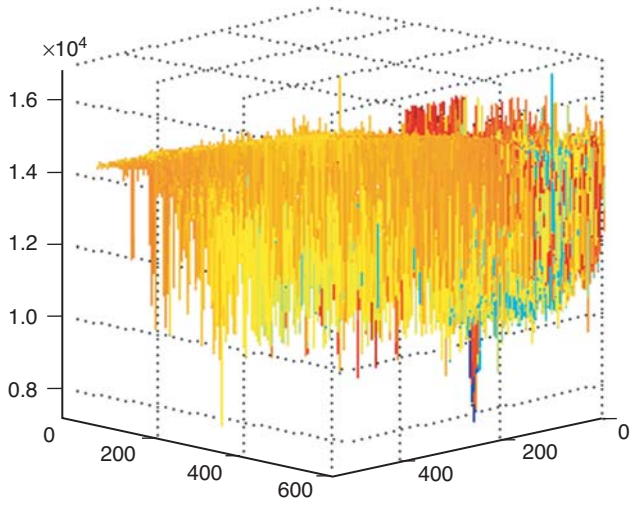

Fig. 7. An example of the QWIP output with an average 13,600 counts and several individual pixels reaching full well depth of 16,384. Lateral units are numbers of pixels and the vertical axis represents signal counts.

flux is expected to increase linearly with integration time. This is indeed the case, as shown in Fig. 8. The measurements are taken with the flux input at room temperature. Output increases linearly with integration time up to 30 ms at the fixed input, as shown in Fig. 8(a); Fig. 8(b) gives a quantitative measurement on the deviation of measurement from the linear fitting. The maximum deviation from linearity is 2.7 percent, occurring at the shortest integration time of 2 ms. At a long integration time, deviation from linearity becomes negligible.

B. Miricle® Bolometer

A microbolometer from Thermoteknix is the second IR camera characterized [4]. The bolometer for IR signal detection is based on resistance sensitivity to thermal variation of an object, and its spectral response falls in the band of 7 to 14 μm. It is uncooled and operates at room temperature, with a response time of 7 ms. Operating at room temperature, noise becomes a major limitation. The bolometer is, therefore, not expected to perform as well as the QWIP for our application. The 384×288 pixel detector array of the bolometer IR camera has an overall area of 13.4×10.1 mm^2 with each pixel 35×35 μm^2

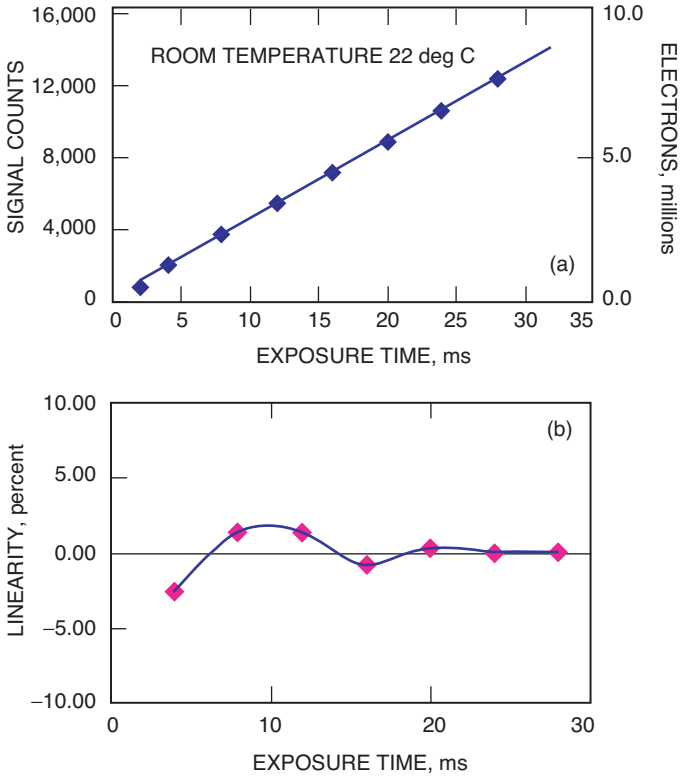

Fig. 8. Linearity on integration time for the input flux at room temperature: (a) signal counts versus integration time and (b) deviation of measurement from linear fitting.

in size. Compared to the QWIP camera with a pixel size of 25×25 μm^2, the bolometer resolution is coarse. On the other hand, the bolometer camera, similarly to the QWIP, has a 14-bit dynamic range. For comparison, the Miricle® bolometer is characterized for its nonuniformity, low signal response, and saturation limitation for a high signal input.

1. Pixel-to-Pixel Nonuniformity. The performance of the QWIP is limited by pixel-to-pixel nonuniformity because of its low noise and high sensitivity. However, the noise level of a bolometer is high and the sensitivity is relatively low; consequently, pixel-to-pixel nonuniformity becomes a secondary issue for the bolometer as compared with its noise. Figure 9 is an example of the Miricle® bolometer detector-array response to room temperature thermal exposure without its lens on. The nonuniformity is 0.04 percent, less than that of the QWIP IR camera discussed in the previous subsection.

2. Low-Temperature Response. To clarify and understand the limitation of the Thermoteknix bolometer response to a low signal input, a liquid nitrogen test is performed with the bolometer. The results are shown in Fig. 10. The average output count is 3200 with variation from 0 to 5000 counts. The IR imaging using the bolometer at low temperature/signal input is limited by noise. In this regard, the bolometer performance is inferior to that of the QWIP camera.

3. Saturation and Dynamic Range. The dynamic range of the Thermoteknix bolometer is also examined for its relevant application in the laboratory test bed. The low end of the dynamic range

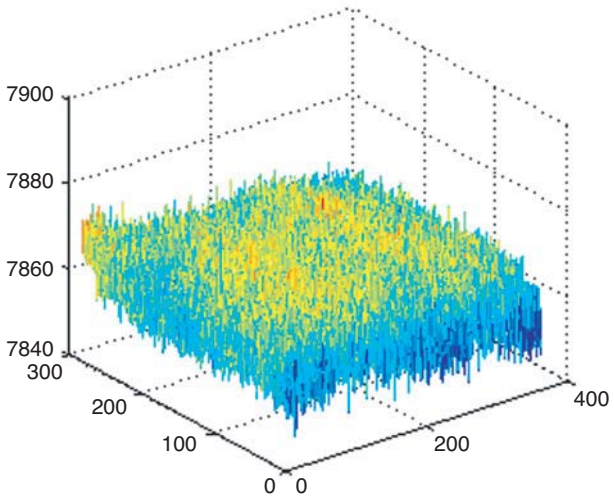

Fig. 9. An example of the nonuniformity of the Miricle® bolometer at a room temperature of 24 deg C. Lateral units are numbers of pixels and the vertical axis represents signal counts.

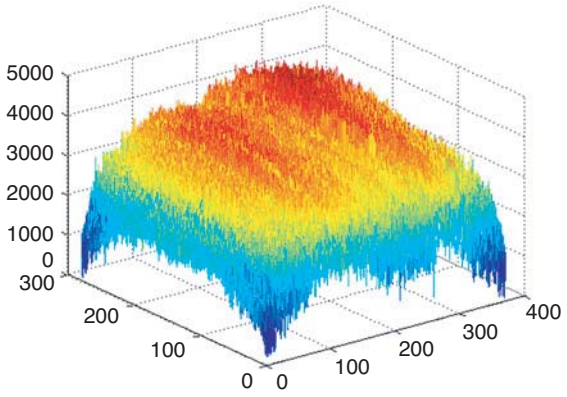

Fig. 10. The Thermoteknix bolometer output when imaging at liquid nitrogen. Lateral units are numbers of pixels and the vertical axis represents signal counts.

of the bolometer response is limited by noise, and its high end is clipped by saturation at a high signal level input. The output of the bolometer in terms of counts for a 14-bit range is measured for various IR source emission temperatures, and the results are plotted in Fig. 11. Output counts increase with increasing IR emission level and start to saturate above 200 deg C of IR source emission temperature. The count variation per degree of emission temperature change is 53 counts/deg C for the bolometer, three times smaller than that of the QWIP at a 16-ms integration time. In this test, the Miricle® bolometer is less sensitive to emission temperature variation than is the QWIP camera.

Based on its operation features, the bolometer appears to be a good candidate for IR Earth tracking within a very short range of mission; it has the advantage of simplicity and low cost for implementation. For long-range missions and a mission requiring large dynamic range, the QWIP or other more advanced IR cameras meet the requirements more closely.

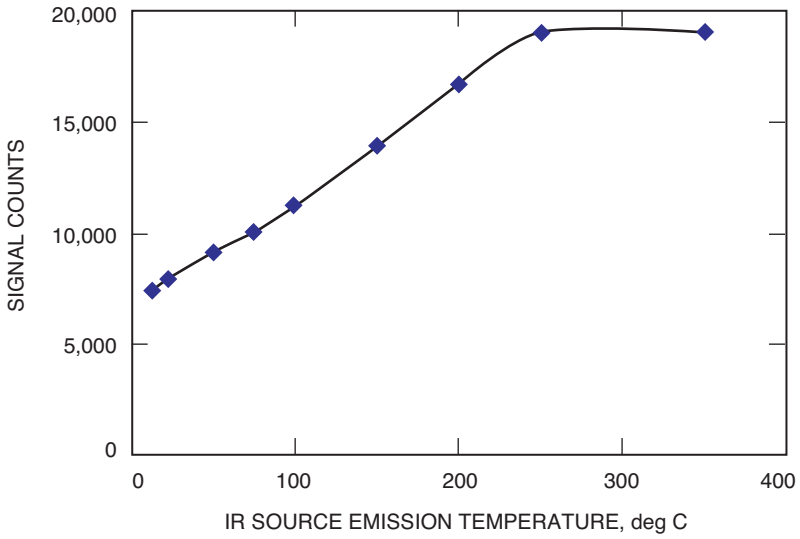

Fig. 11. Signal output of the Miricle® bolometer versus input from an IR source.

IV. Range Emulator from 0.38 to 24 AU

Figure 2 is the schematic of the laboratory emulator setup, where range emulator mirrors 1 to 8 emulate distances from 0.1 AU to beyond 40 AU. The IR emission can be adjusted by IR source emission temperature. Based on the setup, a series of laboratory emulator images ranging from 0.38 to 24 AU with an IR source emission temperature of 150 deg C and an integration time of 16 ms is captured by the QWIP. The results are presented in Fig. 12, together with corresponding theoretical modeling. The resemblance between the laboratory measurement and theoretical modeling appears to be good. In the laboratory emulator, IR source emission temperature is fixed (150 deg C). With increasing range, the signal level fades along with reduced image size. This is illustrated in IR image evolution over the range presented in Fig. 12(a) (0.38 AU) through Fig. 12(e) (6 AU) for a telescope aperture of 25 cm, where a constant background contribution from the surroundings is subtracted. A blurring effect also becomes dominant with increasing range.

By increasing the telescope aperture size, blurring impact can be alleviated, and an image can be recovered close to the Earth's actual angular size. Signal level is also boosted when a larger aperture is used. This is demonstrated in Figs. 12(e) and 12(f), which are imaged at the same range of 6 AU but with different telescope apertures of 25 and 50 cm, respectively. Increasing the aperture size from 25 to 50 cm for long range allows the IR image to be detected at 12 AU, Fig. 12(g), and 24 AU, Fig. 12(h), with the fixed IR source emission temperature. To get better detection of an IR image at longer range, two options are increasing the IR source emission and improving IR camera sensitivity.

For a quantitative comparison, Fig. 13 plots the measured emulator FWHM size against the theoretical modeling. Laboratory measurement apparently agrees well with the theoretical modeling.

V. Emulating IR Earth Nonuniformity

In the last section, the IR source used to emulate the IR Earth image on the test bed had a uniform emissivity across the cross section. With increasing distance, the image becomes smaller and gets blurred. The radial symmetry of the source object, however, is retained over different ranges while the image is blurred by the diffraction effects associated with a finite telescope aperture size.

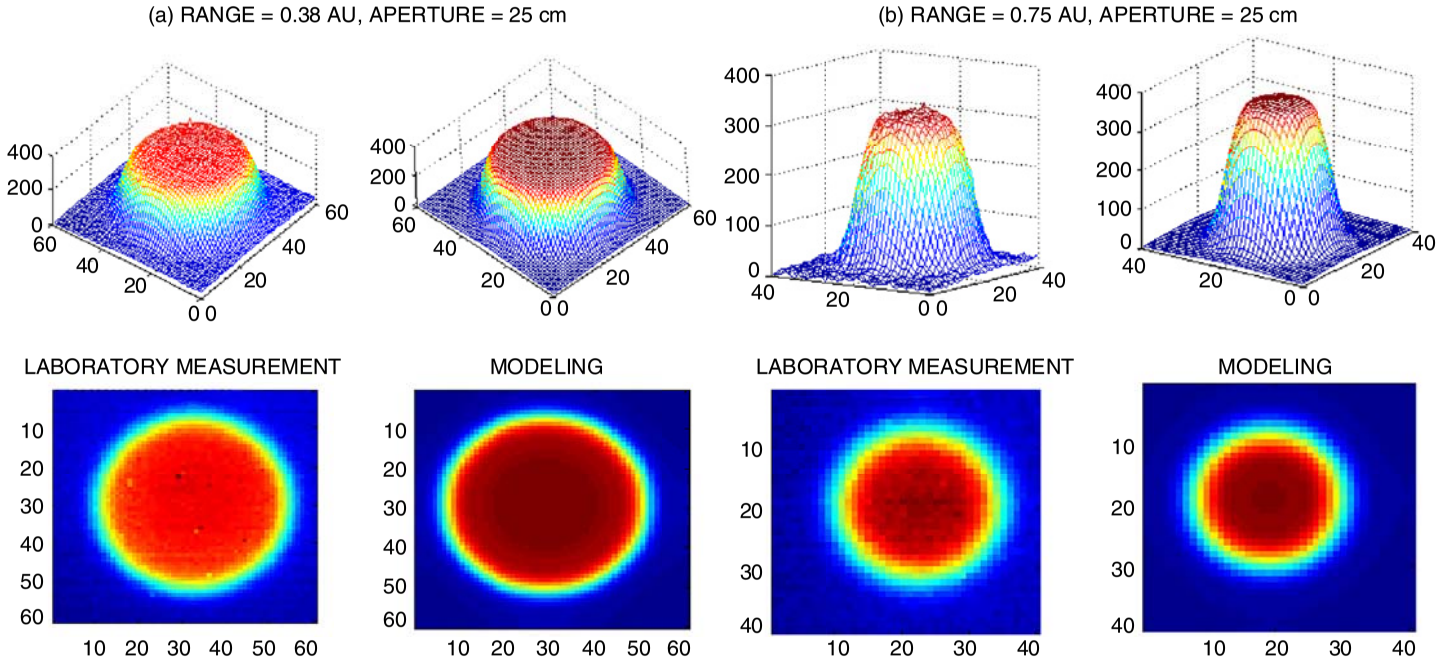

Fig. 12. Comparison of IR Earth laboratory emulator images with the corresponding theoretical modeling. Lateral units are numbers of pixels and the vertical axes represent signal counts.

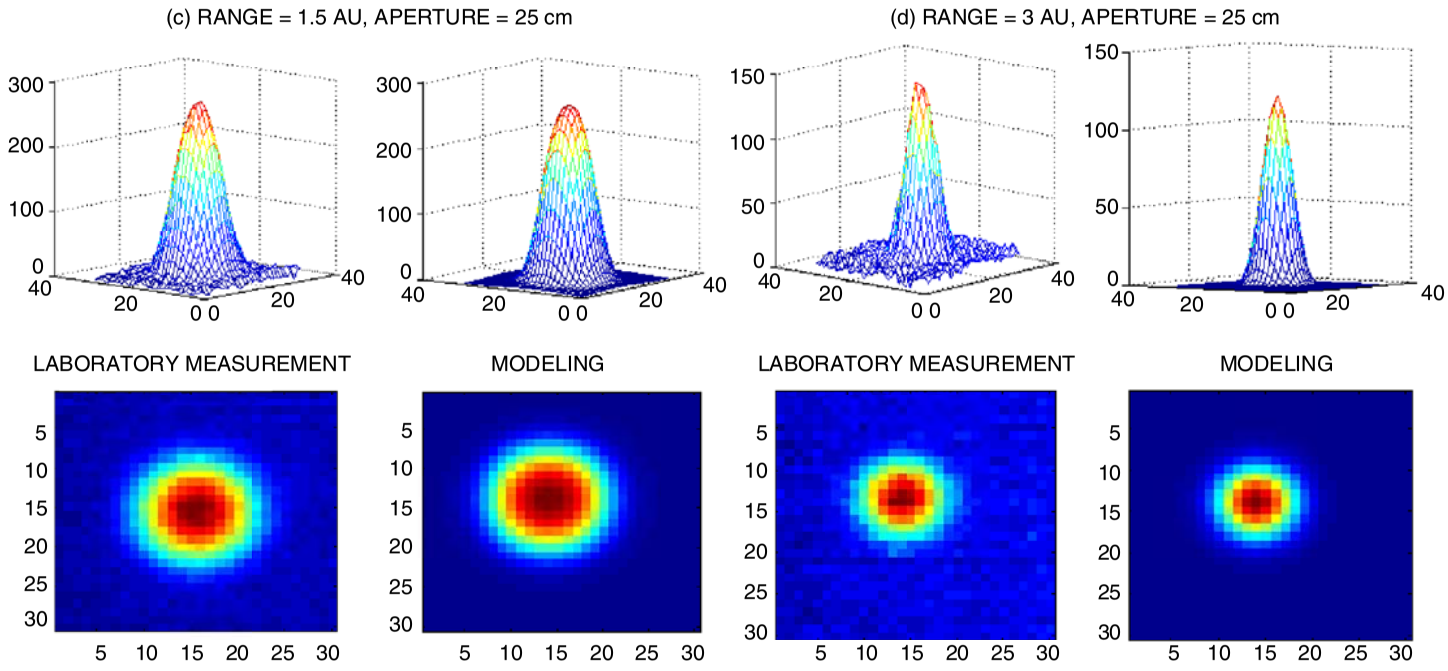

Fig. 12 (continued).

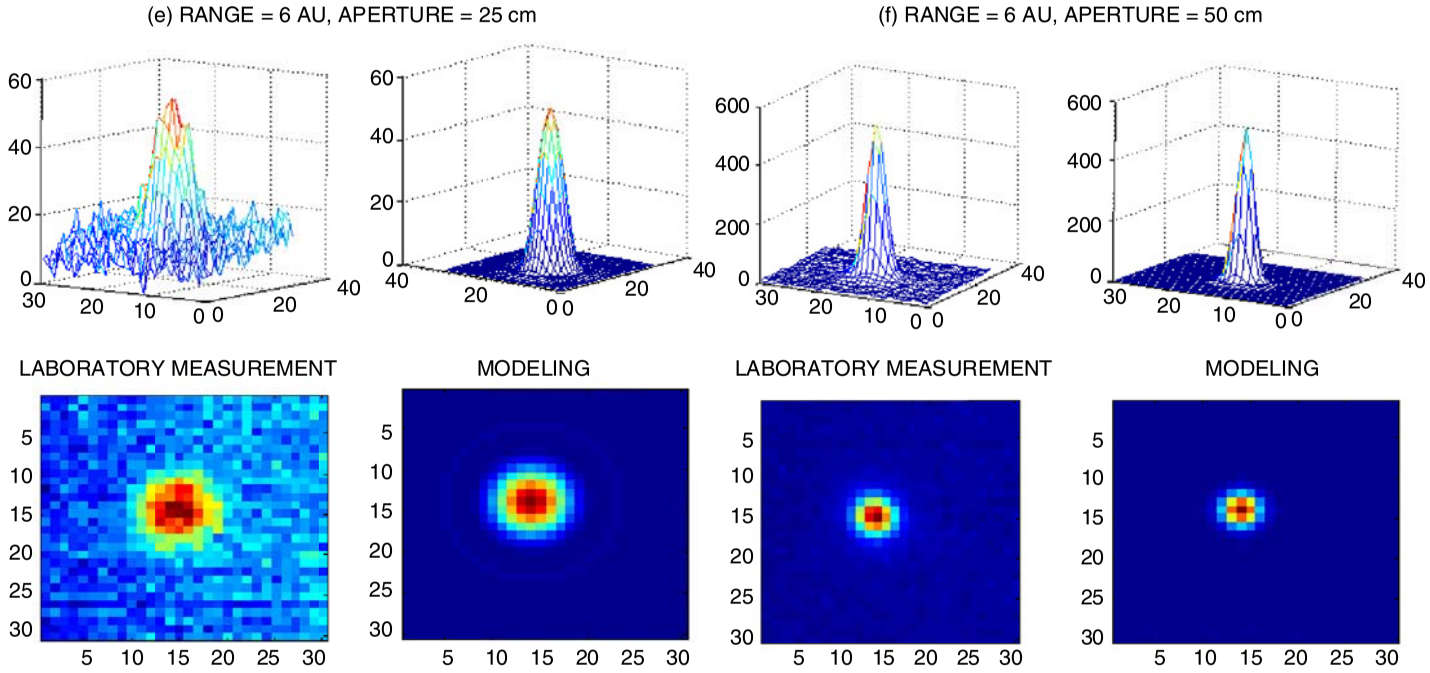

Fig. 12 (continued).

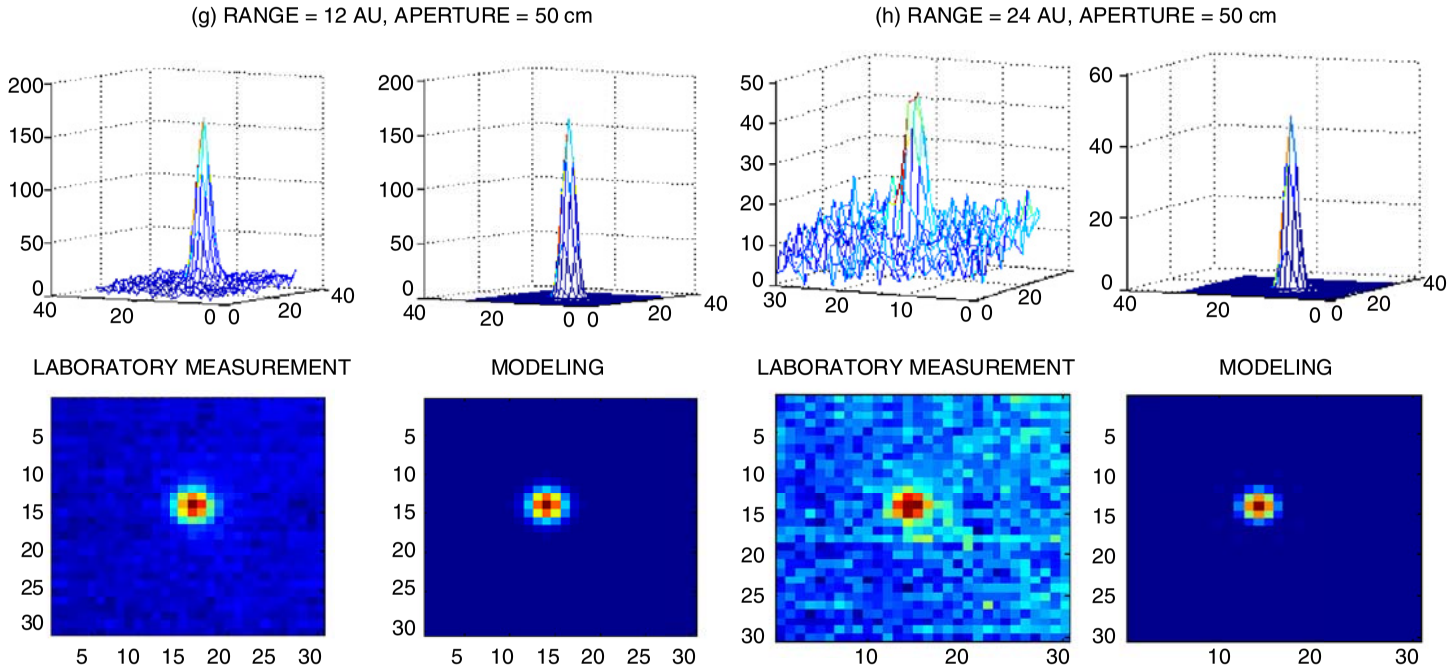

Fig. 12 (continued).

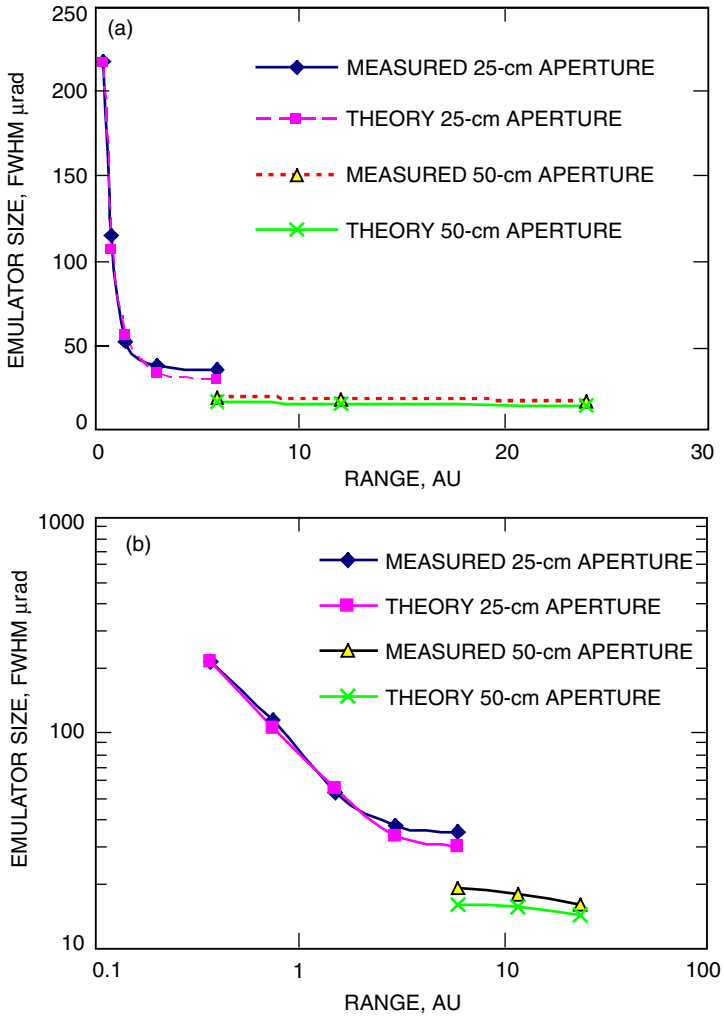

Fig. 13. Comparison of laboratory emulator IR Earth image size with the corresponding theoretical modeling: (a) linear scale and (b) log scale.

The temperature on the surface of the Earth is not uniform, varying from the poles at −20 deg C to well over 40 deg C around the equator. Accordingly, the IR emission level across the Earth surface varies, producing an emissivity differentiation over the IR Earth image with a peak-to-valley variation as great as 6. Seen from a spacecraft, the Earth IR image is neither uniform nor symmetric. To simulate such IR Earth nonuniformity in the laboratory test bed, e.g, for the purpose of verifying the centroiding algorithm, an IR mask is made and placed in front of the IR source (Fig. 14). The mask is a simple crescent shape. This is not a characteristic of a true IR Earth image, but for our purpose here, it provides a strong bias in the nonuniform image. The mask is made from sun-filter materials, creating differential transmission of the IR source image. Figure 15 shows an evolution of the nonuniform IR image over the range captured by the QWIP using the setup of Fig. 14.

At a range of 0.2 AU, Fig. 15(a), nonuniformity of the image has a ratio of 6 to 1. As the simulated range increases, the image gets blurred. Asymmetry of the simulated IR Earth image is reduced greatly at 2 AU, Fig. 15(b), and is further reduced at 3 AU, Fig. 15(c). Beyond the 4-AU range, Figs. 15(d) through 15(f), the nonuniformity of the simulated Earth image is washed out by blurring, and the IR images become relatively symmetric. Earth approaches a point source when the spacecraft is far away, although some bias equivalent to a fraction of the Earth diameter is admittedly retained.

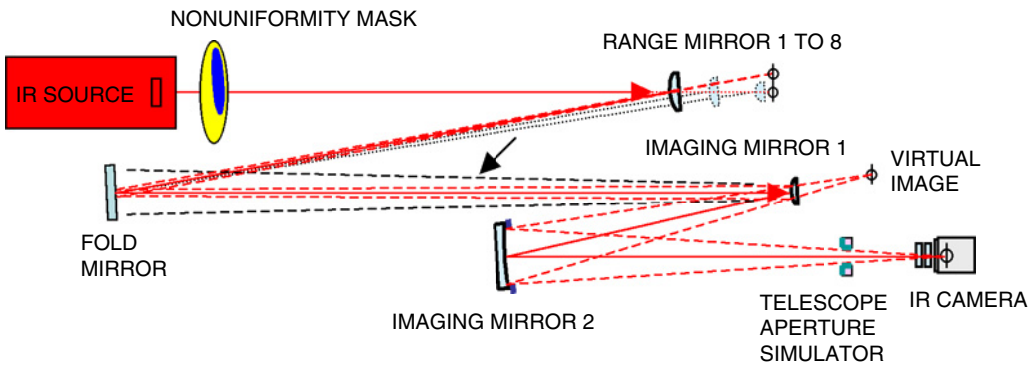

Fig. 14. Setup for simulating Earth nonuniformity.

VI. Centroiding Accuracy

One of our goals with the test bed is to establish/verify centroiding accuracy in identifying the Earth center. The objective of IR Earth tracking for optical communications is to locate the Earth center from a detected IR Earth image. Once the Earth center is derived, the location of the optical receiver can be computed from the information of the established Earth time zone.

Any detected image experiences distortion. The IR Earth image captured by the IR camera is distorted by various imperfections. Camera detector noise is one source that deforms the IR Earth image, introducing errors in finding the Earth center. To assess the effect of the array detector's random noise on centroiding accuracy, preliminary analysis on statistical centroiding error for the simulated Earth image obtained with the emulator is performed.

For symmetric images, the center of the simulated Earth image can be obtained either by the center-of-mass approach or by an edge-detection algorithm. For measuring the centroid, the edge-detection algorithm is employed. This is because Earth, with a mean temperature of 280 K and surrounded by a cold universe, has a sharp edge. In the 4- to 5-AU range, the edge-detection algorithm has advantages over the center-of-mass approach in identifying the Earth center due to the presence of Earth IR nonuniformity.

To estimate centroiding error, we need first to identify the center of the laboratory-simulated IR image. This is done by collecting a thousand IR images for a fixed signal level and range. The center of the emulated Earth image is derived by taking the mean position of the images. The center of each individual image is obtained by the edge-detection algorithm. An example of a detected edge and a calculated center is given in Fig. 16. Due to the statistical nature of the detector, the computed center of the laboratory measurement varies from image to image. This is shown in Fig. 17, where the x- and y-coordinates of the image centers scatter around the mean. Defining the centroiding error as the maximum computed center deviation among the thousand images from the mean, the centroiding error is evaluated for a fixed signal level and range. Figure 18 plots measured centroiding errors for a series of signal levels (in terms of IR source emission temperature) at ranges of 2 AU and 4 AU.

With a simulated receiving telescope focal length of 5 m and the QWIP's pixel size of 25×25 μm^2, each detector pixel corresponds to 5 μrad. This yields an expected 8.4 pixels for the laboratory-simulated IR Earth image at 2 AU. The actual measured image, however, is 10 pixels in size (Fig. 18). The reason for the difference is blurring due to the Airy pattern of the simulated 50-cm telescope aperture in the laboratory test setup. Similarly, 4.2 pixels are expected for 4 AU in the laboratory-simulated IR Earth image of Fig. 18. Blurring of the telescope with a 50-cm aperture size increases the image size to 6 pixels.

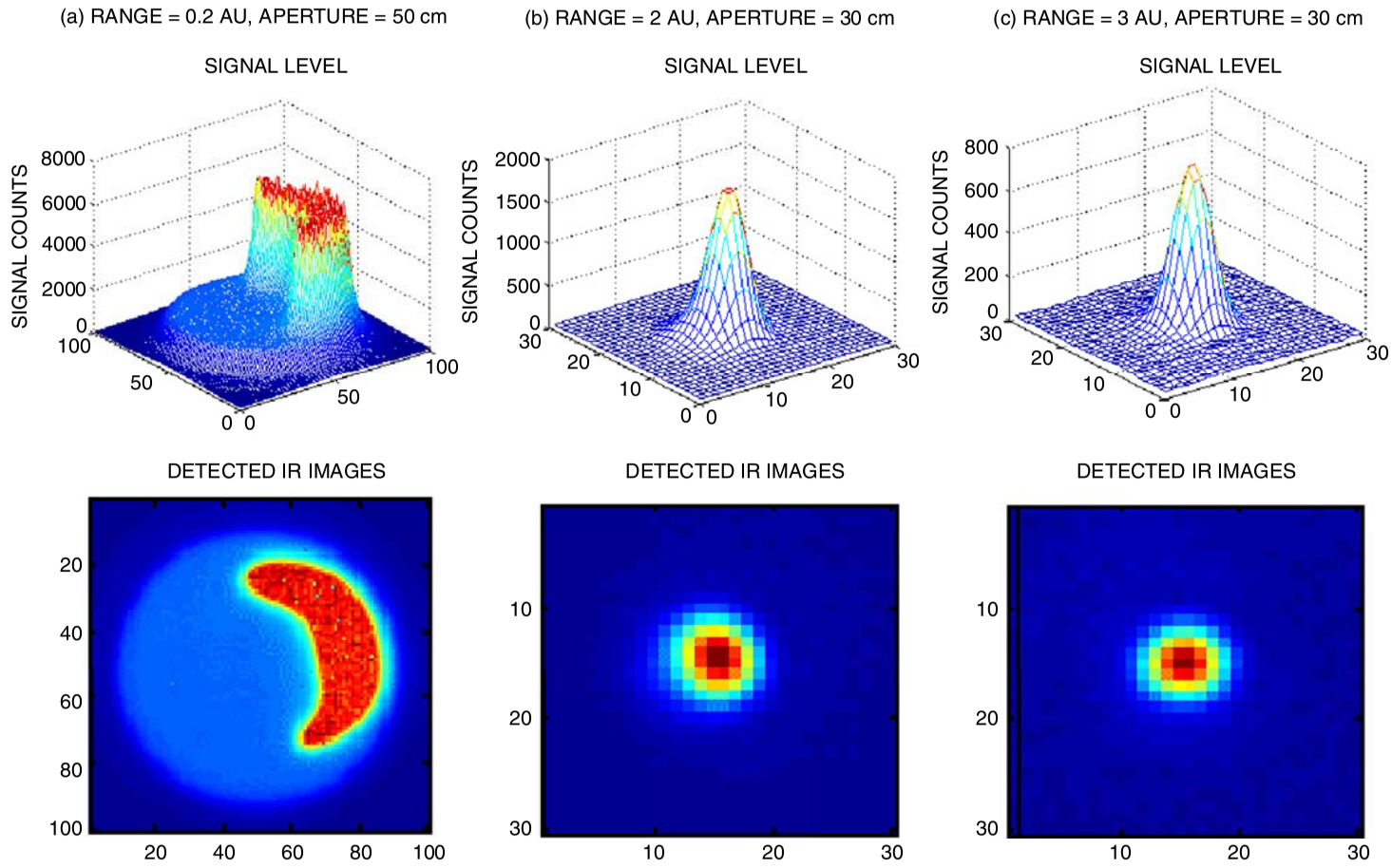

Fig. 15. Evolution of nonuniformity over range. Lateral units are numbers of pixels.

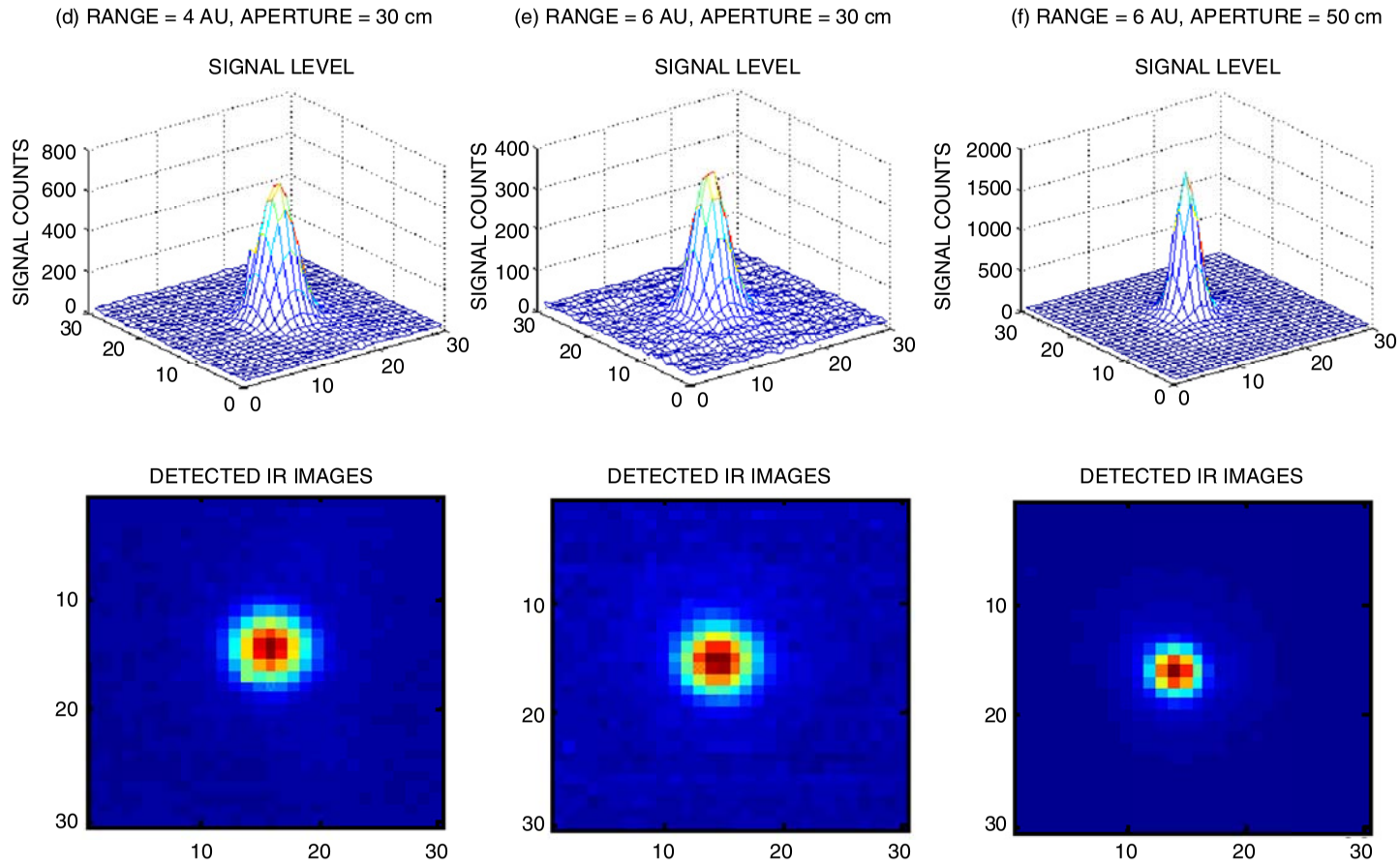

Fig. 15 (continued).

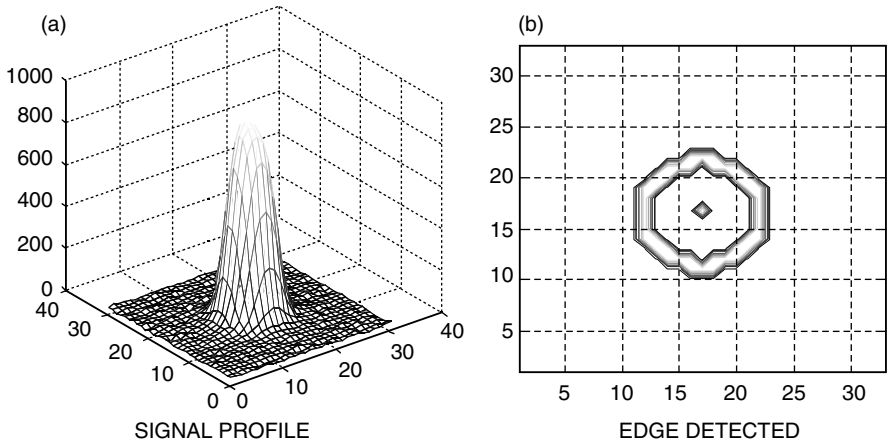

Fig. 16. Example of (a) a laboratory-simulated image and (b) a detected edge at 2 AU with an IR source emission temperature of 150 deg C. Lateral units are numbers of pixels and the vertical axes represent signal counts.

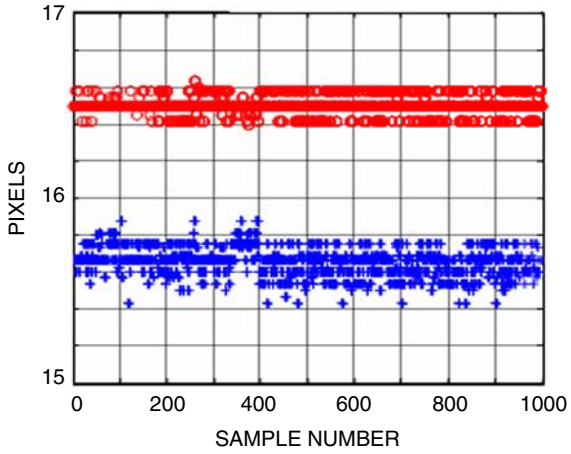

Fig. 17. Statistical distribution of the detected image center at 4 AU with an IR source emission temperature of 125 deg C. The circle and plus symbols represent image center x- and y-coordinates, respectively, in the pixel.

As shown in Fig. 18, the centroiding error for a uniform simulated Earth image decreases with increasing IR source emission temperature or signal level and decreases with increasing image size. These results are consistent with the theoretical analysis. The impact of random detector noise is reduced with increasing signal level.

VII. Conclusion

As a part of feasibility analysis for the IR Earth-tracking experiment, we have investigated characteristics of the QWIP camera. Operating at 67 K, the QWIP has low dark current and can be a potential candidate for an onboard flight tracking receiver used in optical communications with IR Earth tracking. The QWIP has excellent linearity versus integration time, which can be tailored for different ranges/signal levels to accommodate large dynamic ranges. Currently, the QWIP's nonuniformity limits its performance at low and high signal levels, since it was designed and calibrated for imaging around room temperature. By extending nonuniformity calibration to various signal levels, the QWIP is expected to perform well across all its dynamic ranges.

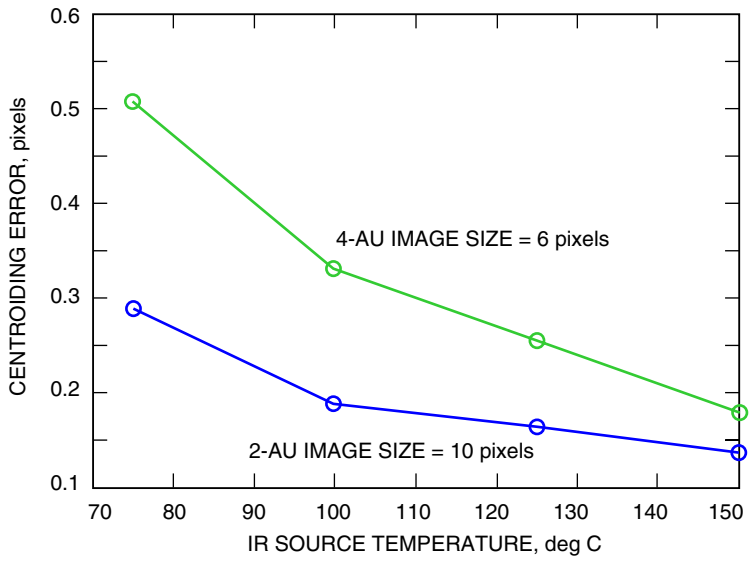

Fig. 18. Centroiding errors versus IR source emission temperature for ranges of 2 and 4 AU.

An emulator test bed for IR Earth tracking was designed and evaluated. IR Earth images were successfully emulated from 0.38 to 24 AU. Laboratory test-bed simulated images compared well with the theoretical modeling. This accomplishment lays the groundwork for further experimental study on IR Earth tracking.

Moreover, some aspects of IR Earth nonuniformity have been simulated on the laboratory test bed. Within short ranges, an IR Earth image is shown to be dominated by the nonuniformity. As the range increases beyond 4 AU, an IR Earth image is blurred by diffraction effects of a finite receiver telescope aperture size, and the nonuniformity is washed out by blurring. An IR Earth image approaches characteristics of a point source when the flight terminal is far away. This implies that different algorithms will be suitable for IR Earth detection and centroiding at different ranges or terminal apertures.

Lastly, preliminary analysis on centroiding accuracy was conducted on data acquired with the test bed. The analysis indicates that, with the edge-detection method, centroiding accuracy improves with increasing image size and signal level. Extensive quantitative analysis on this subject needs to be pursued further.

Future test-bed work will include development of a background subtraction technique. In an interplanetary mission, the IR Earth signal may be very weak and overwhelmed by the optical background emission. The background subtraction technique needs to be developed if the optical system on the spacecraft and the area surrounding the IR camera are not cooled or where a cooling scheme is not effective in suppressing the stray light effects. The next phase of the experiment may also involve a field experiment to detect distant IR images of Mars and Venus, as well as emulation of real-time IR Earth tracking on the laboratory test bed.

Acknowledgments

The QWIP camera used in our experiment was provided by the Infrared Photonics Group at JPL, and the work done here was sponsored by the JPL Research and Development Program.

References

[1] A. Biswas, M. Wright, J. Kovalik, and S. Piazzilla, "Uplink Beacon Laser for Mars Laser Communication Demonstration (MLCD)," *Proc. SPIE 5712*, vol. 93, pp. 93–100, 2005.

[2] H. Hemmati, Y. Chen, S. Lee, and G. G. Ortiz, "Earth-Image Tracking in the IR for Deep Space Optical Communications", presented at LEOS-2005, Sydney, Australia, October 23–27, 2005.

[3] S. D. Gunapala, S. V. Bandara, J. K. Liu, S. B. Rafol, and J. M. Mumolo, "Large Format Long-Wavelength Narrow-Band, Multi-Band, and Broad-Band QWIP Focal Plane Arrays," *SPIE*, vol. 5234, pp. 272–286, 2004.

[4] Thermoteknix Systems Ltd., Cambridge, United Kingdom, www.thermoteknix.com.